Mechanics of Materials 16 (1993) 239–247
Elsevier

Numerical simulation of inclined chute flows of monodisperse, inelastic, frictional spheres

Otis R. Walton

Lawrence Livermore National Laboratory, Livermore, CA, USA

Received 28 April 1992; accepted 7 August 1992

Molecular-dynamics-like simulations are utilized to map regions of flow parameter space where steady flows occur for monodisperse assemblies of inelastic, frictional spheres, flowing down frictional, inclined planar surfaces. The trajectory-following technique utilizes nearly-rigid particles interacting via contact forces and gravity. Energy losses in the simulations occur only via displacement-dependent hysteretic loading/unloading paths and sliding friction. Initial scoping calculations are examining flows on an incline tilted 17° from the horizontal, determining the boundaries of various flow regimes. Assemblies of inelastic spheres with interparticle friction coefficients less than the tangent of the inclination angle accelerate unboundedly. Those with friction coefficients somewhat greater than the tangent of the inclination angle develop steady velocity and density profiles for a variety of flow depths but result in arrested flow for coefficients of friction greatly exceeding the inclination angle tangent (e.g., by more than a factor of 2). Conversely, a significant range of inclination angles that will result in steady flows for a given set of assembly properties, is expected to exist.

1. Simulation technique

The calculations reported here are carried out for a fixed number of spherical particles on an inclined, frictional, planar surface. The calculational space is bounded: on four sides with stationary periodic boundaries; on the bottom by the frictional plane; and the top surface is free. The simulations are initiated with the spheres placed randomly in the region above the inclined surface, distributed over a height so that the initial solids packing is 0.4 or less. The particles are assigned small random velocities, and they are also given an initial mean group velocity down the incline (usually at a speed slightly faster than the expected steady-state speed). No initial gradients in velocity or density are assigned to the assembly. For ease of modeling, the x-axis is aligned with the lower (inclined) plane and gravity is then "tilted" to provide the driving force for the flow. The dynamical equations are "turned on" and the flow is allowed to develop. Because periodic boundaries are used in the direction of flow, only "steady-state" conditions are physically meaningful. Thus, the system is allowed to "evolve" until parameters such as the mean flow velocity and the time averaged velocity and density profiles remain constant in time. Once a steady condition is achieved, time averages are accumulated. In these simulations there are no side wall effects and the total number of particles per unit area is fixed (an input quantity). During the simulation we can calculate the mean flow velocity, mass flux, density and velocity profiles and other "internal" flow parameters.

These simulations differ somewhat from a typical chute flow experiment wherein particles are usually supplied through an opening of fixed area, producing a flow with a fixed mass flow rate. The mass-per-unit-area for such flow can be measured

Correspondence to: Dr. O.R. Walton, Energy Program, L-207, Lawrence Livermore National Laboratory, P.O. Box 808, Livermore, CA 94550, USA.

in the laboratory quite readily by "capturing" the flowing material between two rapidly closed gates (Patton, 1985) (providing a simple method to determine the mean flow velocity). Surface velocities are also often measured in laboratory tests, usually using non-intrusive optical techniques such as fiber optics probes or motion pictures. Determination or attainment of "steady-state" is usually restricted in laboratory tests by the physical length of the chute.

Comparisons between the models used here and laboratory measurements of essentially 2-dimensional chute flows (between two vertical walls, one particle diameter apart) have shown good agreement on the velocity and density profiles obtained in near steady-state flows (Drake, 1988; 1992). Comparisons with Couette flow experiments have shown similar good agreement between measured and model calculated stresses in steady shearing flows (Savage and Sayed, 1984; Campbell, 1986; Walton 1990). These comparisons and others give us confidence that the behavior generated by these models is very much like the behavior of real spheres in physical tests. Comparisons with kinetic-theory based predictions of granular flow behavior have also shown reasonably good agreement when the simulations have excluded frictional coupling so as to simulate particles with properties similar to those in the kinetic theories (Lun et al., 1984; Jenkins and Mancini, 1989; Richman, 1989; Walton et al., 1991).

2. Numerical method

The numerical method utilizes a straight forward extension to 3-dimensions of the 2-dimensional contact force models and integration equations of Walton and Braun (1986), (WB model). Explicit integration of Newton's equations of motion is accomplished via the "leap-frog" method for each of 6 degrees of freedom (see Allen and Tildesley (1987)). Since the particles are spherical, only the magnitude and direction of the angular velocity is needed to determine the infinitesimal surface displacements between timesteps (i.e., the information necessary to determine changes in tangential friction forces). For the motion of one sphere in the x-direction and rotation about its x-axis the finite difference equations are:

$$\dot{x}^{n+1/2} = \dot{x}^{n-1/2} + \left(\frac{F_x^n}{m} + g_x \right) \Delta t,$$

velocity,

$$x^{n+1} = x^n + \dot{x}^{n+1/2}\, \Delta t,$$

position,

$$\dot{\omega}_x^{n+1/2} = \dot{\omega}_x^{n-1/2} + \frac{N_x^n}{I_0} \Delta t,$$

angular velocity,

where the superscript, n, refers to the current time step; F_x is the x-component of the sum of all contact forces acting on the sphere; g_x is the x-component of the applied body force (i.e., gravity); m is mass; N is torque; I_0 is moment of inertia, and Δt is the time step. Similar equations are used for the other two directions. The orientations of the individual spheres (e.g., Euler angles) are not needed to determine the forces or the subsequent motion; however, in anticipation of utilizing non-spherical particles in future calculations, and for visualization of particles rolling, the orientation of each sphere is determined in the simulations utilizing a slightly modified form of the quaternion method described by Evans (1977). Details of that implementation will be included in a subsequent paper.

2.1. Normal force

The normal force during contact, F_N, is identical to the WB model:

$$F_N = \begin{cases} K_1 \alpha, & \text{for loading,} \\ K_2(\alpha - \alpha_0), & \text{for unloading,} \end{cases}$$

where α is the "overlap" between the contacting spheres; $K_2 > K_1$; and α_0 represents the relative "overlap" where the unloading force is set to zero (due to inelastic deformation of the surfaces). This normal-force model produces binary collisions with a constant coefficient of restitution given by $e = \sqrt{K_1/K_2}$, independent of the relative

velocity of impact. Experimental evidence for this model, and finite element calculations that this model mimics, are discussed in Walton (1992).

2.2. Tangential force

The tangential friction force is a two-dimensional (surface) extension to Walton and Braun's one-dimensional approximation to Mindlin's (1949) elastic frictional sphere contact force model. In that WB model the effective tangential stiffness of a contact decreases with tangential displacement until it is zero when full sliding occurs. In the present two-dimensional surface model the tangential displacement *parallel* to the current friction force and the displacement *perpendicular* to the existing friction force are considered separately. They are later combined vectorially and their sum is checked against the total friction force limit, μF_N.

The effective tangential stiffness in the direction *parallel* to the existing friction force is given by:

$$K_T = \begin{cases} K_0\left(1 - \dfrac{T - T^*}{\mu F_N - T^*}\right)^{\gamma}, & \text{for } T \text{ increasing,} \\ K_0\left(1 - \dfrac{T^* - T}{\mu F_N + T^*}\right)^{\gamma}, & \text{for } T \text{ decreasing,} \end{cases} \tag{1}$$

where K_0 is the initial tangential stiffness; T is the current tangential force magnitude; T^* starts as zero and is subsequently set to the value of the total tangential force, T, whenever the magnitude changes from increasing to decreasing, or vice versa; γ is a fixed parameter often set to 1/3 to make the model resemble Mindlin's elastic frictional sphere theory, and μ is the coefficient of friction. A value of 1 or 2 for γ more closely mimics the behavior of frictional contacts involving plastic deformation in the contact region (Drake and Walton, 1992).

The implementation of this friction model involves some algebraic and vector manipulation since the direction of the surface normal at contact changes continuously during a typical contact. The simulation model assumes that the displacements from one time step to the next are relatively small. For two spheres in contact we let $\hat{\boldsymbol{k}}_{ij}$ be the current unit vector from the center of sphere I toward the center of sphere J, (i.e., $\hat{\boldsymbol{k}}_{ij} = (\boldsymbol{r}_j - \boldsymbol{r}_i)/|\boldsymbol{r}_j - \boldsymbol{r}_i|$, where $\boldsymbol{r}_i$ is the radius vector for the location of sphere I, etc.). The vector $\hat{\boldsymbol{k}}_{ij}$ is also the unit normal at the contact point between spheres I and J.

The tangential force from the previous time step, $\boldsymbol{T}_{\text{old}}$, is projected onto the current tangent plane,

$$\begin{aligned} \boldsymbol{T}_0 &= \hat{\boldsymbol{k}}_{ij} \times \boldsymbol{T}_{\text{old}} \times \hat{\boldsymbol{k}}_{ij} \\ &= \boldsymbol{T}_{\text{old}} - \hat{\boldsymbol{k}}_{ij}\left(\hat{\boldsymbol{k}}_{ij} \cdot \boldsymbol{T}_{\text{old}}\right). \end{aligned}$$

This projected friction force is normalized to the old magnitude, so that $|\boldsymbol{T}| = |\boldsymbol{T}_{\text{old}}|$, to obtain a new "starting" value for the friction force, $\boldsymbol{T}$, before adding in the effects of displacements during the last time step,

$$\boldsymbol{T} = |\boldsymbol{T}_{\text{old}}/\boldsymbol{T}_0|\,\boldsymbol{T}_0.$$

A unit vector in the direction of this "starting" friction force, $\hat{\boldsymbol{t}} = \boldsymbol{T}/|\boldsymbol{T}|$, is used in several subsequent steps.

The relative surface displacement during the last time step is projected onto the contact tangent plane,

$$\begin{aligned} \Delta \boldsymbol{s}^{n-1/2} &= \Big[\hat{\boldsymbol{k}}_{ij} \times \left(\boldsymbol{v}_j^{n-1/2} - \boldsymbol{v}_i^{n-1/2}\right) \times \hat{\boldsymbol{k}}_{ij} \\ &\quad + r_i\left(\vec{\boldsymbol{\omega}}_i^{n-1/2} \times \hat{\boldsymbol{k}}_{ij}\right) + r_j\left(\vec{\boldsymbol{\omega}}_j^{n-1/2} \times \hat{\boldsymbol{k}}_{ij}\right)\Big]\,\Delta t \\ &\approx \Delta \boldsymbol{r}_{ij} - \hat{\boldsymbol{k}}_{ij}\left(\hat{\boldsymbol{k}}_{ij} \cdot \Delta \boldsymbol{r}_{ij}\right) \\ &\quad + \Big[r_i\left(\vec{\boldsymbol{\omega}}_i^{n-1/2} \times \hat{\boldsymbol{k}}_{ij}\right) \\ &\quad + r_j\left(\vec{\boldsymbol{\omega}}_j^{n-1/2} \times \hat{\boldsymbol{k}}_{ij}\right)\Big]\,\Delta t, \end{aligned}$$

where $\Delta \boldsymbol{r}_{ij} = \boldsymbol{r}_{ij}^n - \boldsymbol{r}_{ij}^{n-1}$ is the change in the relative position vector during the last time step; $\boldsymbol{v}$ is the velocity, and $\vec{\boldsymbol{\omega}}$ the angular velocity, and r the sphere radius, with subscripts i and j indicating sphere I or J, respectively, and Δt is the timestep.

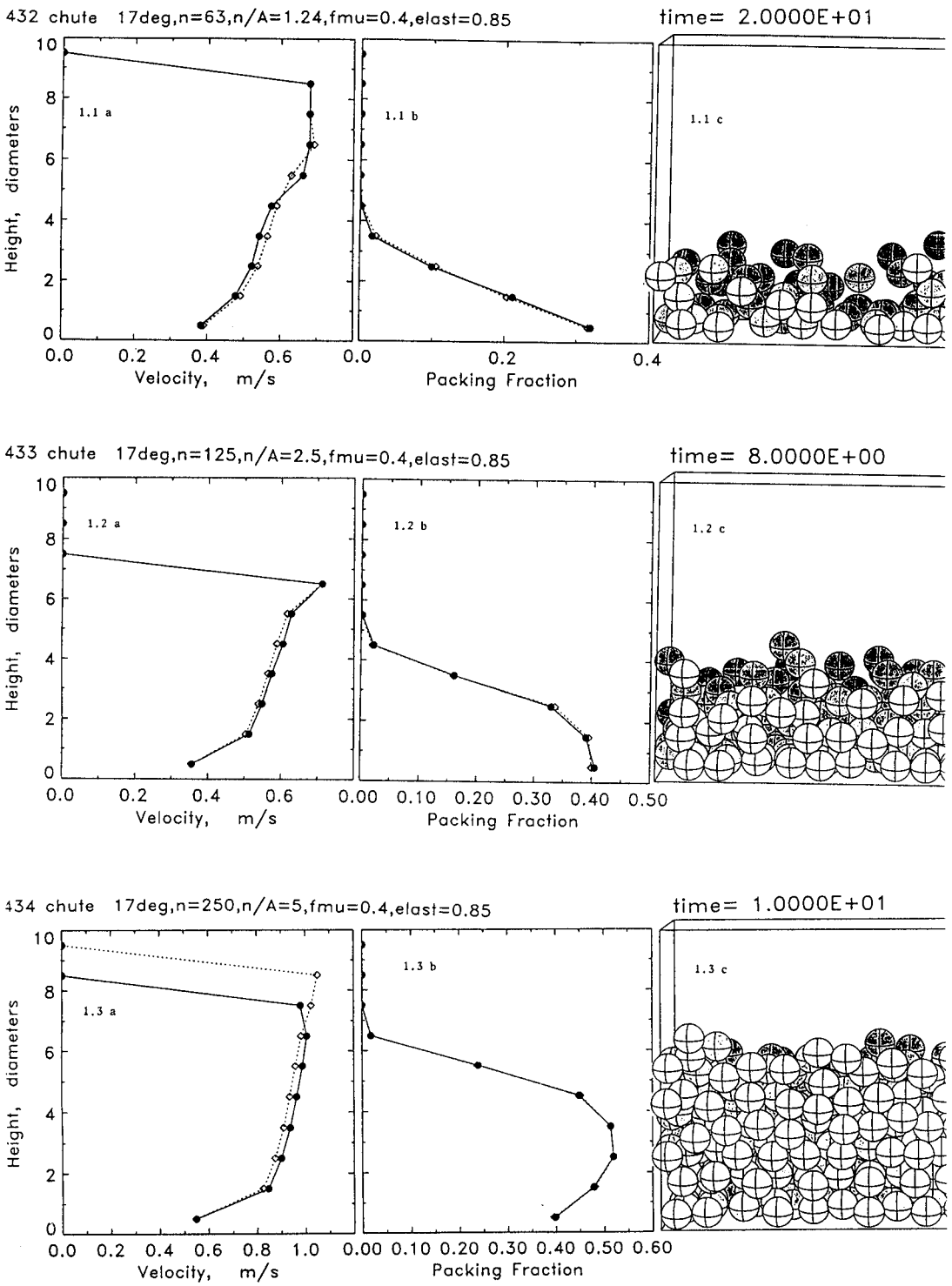

Figs. 1.1–1.6. (a) Velocity; (b) density profiles; and (c) partial configurations of simulation calculations of assemblies of 1 mm diameter spheres on a frictional plane inclined 17° from the horizontal. Solid lines are instantaneous profiles, dotted lines are cumulative time average profiles. Each row is for a different flow depth ($N/\sigma^2 = 1.24$, 2.5, 5, 10, 20, 40 for Figs. 1.1, 1.2, 1.3, 1.4, 1.5, 1.6, respectively). Note the non-shearing and crystalline regions in the deeper flows. (See text for discussion.)

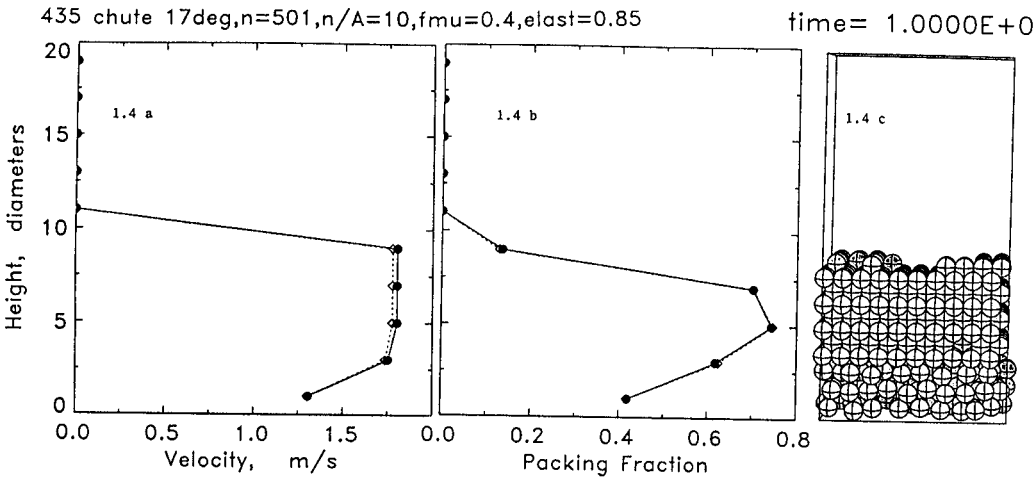

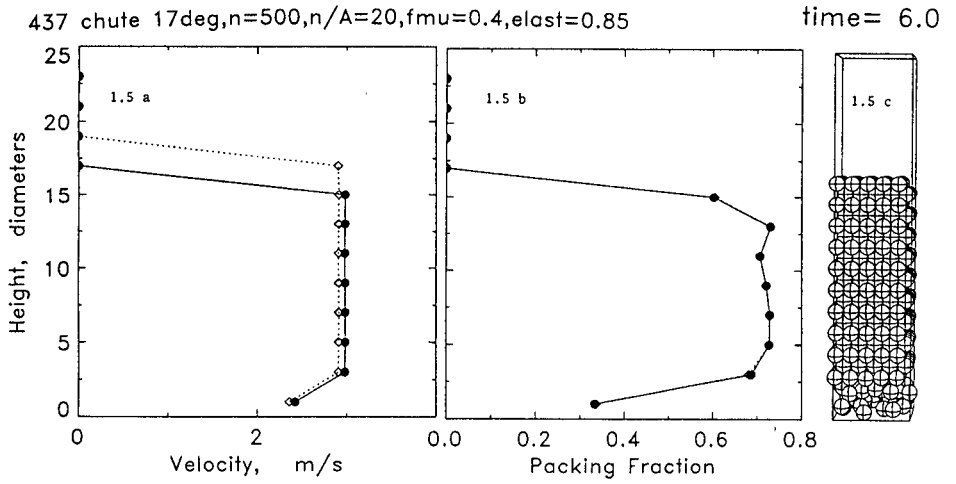

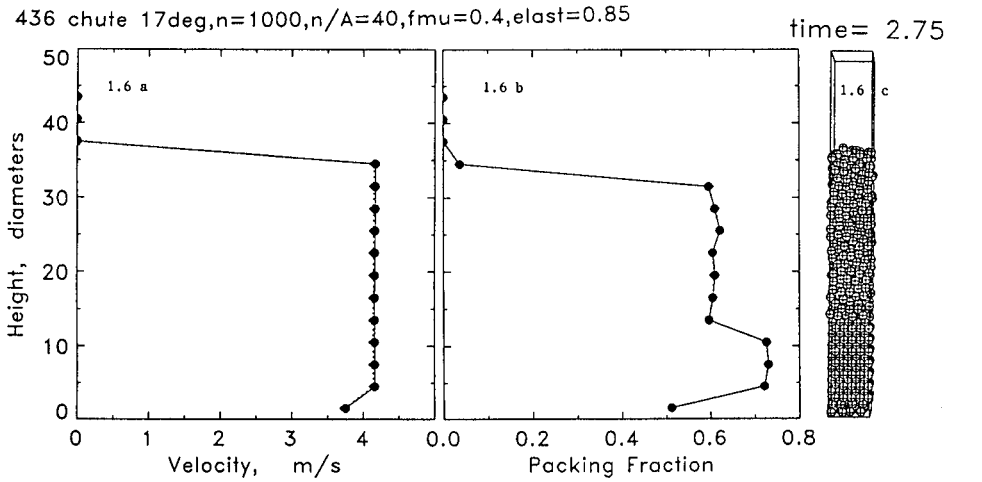

Figs. 1.1–1.6 (Continued).

The displacement parallel to the "old" friction force is

$$\Delta \boldsymbol{s}_{\parallel} = (\Delta \boldsymbol{s}^{n-1/2} \cdot \hat{\boldsymbol{t}})\hat{\boldsymbol{t}},$$

and the displacement perpendicular is

$$\Delta \boldsymbol{s}_{\perp} = \Delta \boldsymbol{s}^{n-1/2} - \Delta \boldsymbol{s}_{\parallel}.$$

The effect of the displacement parallel to the existing friction force is treated almost identically with the 1-dimensional WB model with the exception that the value of T is always positive (since it is the magnitude of a vector in this 2-D model).

If the value of the normal force, F_N, changes from one time step to the next, then the value of T^* in Eq. (1) is scaled in proportion to the change in normal force,

$$T^{*\prime} = T^* \left| F_N^n / F_N^{n-1} \right|.$$

The effective incremental tangential stiffness, K_T, is determined from Eq. (1) with $T^{*\prime}$ substituted for T^*. A new value for the component of the friction force parallel to the old friction force, $\boldsymbol{T}_{\parallel}$, is calculated,

$$\boldsymbol{T}_{\parallel} = \boldsymbol{T} + K_T \, \Delta \boldsymbol{s}_{\parallel}.$$

If both of the conditions $\Delta \boldsymbol{s}^{n-1/2} \cdot \hat{\boldsymbol{t}} < 0$ and $T + (\Delta \boldsymbol{s}^{n-1/2} \cdot \hat{\boldsymbol{t}}) K_T < 0$, are simultaneously true then, in effect, the direction of $\boldsymbol{T}_{\parallel}$ has reversed, and in the model the sign of the effective "remembered" turning point, T^*, is changed (i.e., T^* is replaced by $-T^*$) for the next time step so as to produce a smoothly varying slope using Eq. (1).

Displacement perpendicular to the existing friction force is assumed to have no pre-existing surface strain and is, thus, treated as "new" displacement from the origin with an effective stiffness equal to the value of K_0 in Eq. (1), so that the perpendicular part of the tangential force becomes,

$$\boldsymbol{T}_{\perp} = K_0 \, \Delta \boldsymbol{s}_{\perp}.$$

The new tangential force is tentatively set equal to the vector sum of $\boldsymbol{T}_{\parallel}$ and $\boldsymbol{T}_{\perp}$,

$$\boldsymbol{T}' = \boldsymbol{T}_{\parallel} + \boldsymbol{T}_{\perp}.$$

This value is checked to ensure that it does not exceed the friction limit, μF_N, and if it does, it is scaled back so its magnitude equals that limit.

This tangential force model calculational procedure appears somewhat complex; however, it is quite straight forward to implement in standard Fortran. When the exponent, γ, is set to zero, the model becomes linear. The force–displacement curves generated in this linear case for a series of complex 2-dimensional paths have been checked against the linear 2-dimensional contact model in Cundall and Strack's TRUBALL code (1979a,b), producing essentially identical results with the two models (Trent and Walton, 1987).

3. Results

A variety of flow depths (e.g., number of particles per unit area) and material properties have been examined in simulation calculations of flow down a plane inclined at 17° from the horizontal. We found that for all cases when the coefficient of friction, μ, is less than the tangent of the angle of inclination, then the entire assembly of spheres simply accelerates unboundedly (as might be expected). Similarly, very sparse flows, (i.e., those with only 0.5 particles per diameter squared area), also accelerated unboundedly as the individual spheres rolled down the incline with little or no interaction between them. Flows with between one and two particles per unit area arrive at steady-state velocities that are slower than other flow depths. The mean velocities of the simulated flows tended to increase as the number of particles per unit area increases. Shallow flows (i.e., those with fewer than 5 particles per unit diameter squared surface area) usually exhibit monotonically increasing velocity profiles. Deeper flows often exhibit a non-shearing region riding over the top of a relatively thin shearing layer. The shallowest flows (fewer than 2.5 per unit area) exhibit monotonically decreasing density profiles with height above the incline. Intermediate depth flows exhibit a maximum solids fraction somewhere inside the flow region, while the deepest flows exhibit an essentially uniform (random close packed or crystal) non-shearing region above a

lower density shearing region. Figures 1.1 through 1.6 summarize the results of a series of calculations for spheres with a coefficient of restitution of 0.85 and an interparticulate friction coefficient of 0.4 and an identical value for the coefficient of friction with the lower plane. View a is the velocity profile, b is the density (packing fraction) profile, and c is a snapshot of a portion of the cell for Figs. 1.1 through 1.4 and shows the entire calculational cell for Figs. 1.5 and 1.6. The spherical particles in these simulation calculations had a diameter of 1 mm, a mass of 1.492×10^{-6} kg. Gravitational acceleration was assumed to be 9.8 m/s^2. Values in the figures are stated in MKS units; however, it is quite often convenient to utilize non-dimensional quantities. The most natural non-dimensional units for such flows seem to be: time, $t^* = t\sqrt{g/\sigma}$; length, $l^* = l/\sigma$; and mass, $m^* = m/m_p$ where m_p is the mass of a single particle. Such a selection of non-dimensional units would make non-dimensional velocity, $v^* = v/\sqrt{g\sigma} \approx 10.1v$, and 'spring' stiffness, $K^* = K\sigma/mg \approx 68.4K$.

The unusual crystalline non-shearing regions for flow depths of 10, 20 and 40 are probably more pronounced than would be typical in a physical test for a number of reasons. First, all of the spheres in the simulations are exactly the same size. Second, the inclined plane has no *roughness*; it is perfectly smooth, though frictional. Finally, the calculational space is quite small, being only 5 or 10 particles across. All of these factors increase the likelihood of crystals forming; however, recent personal observations in the laboratory by the author and various articles in the literature such as MacRae and Gray (1961) and Owe Berg et al. (1969) suggest that the appearance of crystalline regions in assemblies of identical spheres may not be that unusual, especially if "appropriate" deformation occurs in an initially random assembly.

The propensity to form crystalline regions is much more pronounced in two-dimensions than in three and such crystallizations have often been seen in past simulation calculations (see for example Walton and Braun (1986)). More recent two-dimensional simulations by Zhang and Campbell (1992) have explored transitions between fluid-like shearing regions and glass-like or crystalline solid-like regions in simulations of Couette flow.

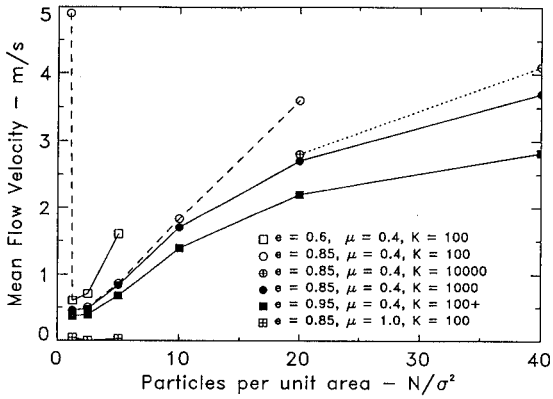

Fig. 2. Mean velocity versus flow depth for simulations of gravity flow of 1 mm diameter spheres on a 17°, frictional, inclined plane.

Figure 2 shows how the mean flow velocity varies with the number of particles per unit area and with material properties such as the coefficient of restitution and the coefficient of friction. Interestingly, the more elastic particles flow slower and have a deeper shearing layer at the bottom than do less elastic particles.

Analysis and interpretation of these flows is still in progress. The ability of a flowing layer to dissipate energy appears to be intimately related to the characteristic depth of shearing that develops. The slowest flows exhibit shearing throughout their height. As the flows get deeper, the thickness of the shearing layer tends to decrease. Thus, a smaller fraction of the total bed tends to be experiencing energy-dissipating inelastic collisions and frictional sliding. Consequently, deep assemblies flow faster than corresponding shallow assemblies. The fast flowing deep layers may have significant implications for long run-out landslides and avalanches.

The total energy loss is a result of a combination of both frictional sliding and collisional losses. However, a simplistic qualitative interpretation of the calculated flow behavior can be made emphasizing the energy losses due to collisions. More-elastic particles produce slower steady-state velocities than do less-elastic particles. These

more-elastic particles can propagate kinetic energy from the bottommost rolling layer deeper into the assembly above; thus, producing deeper shearing layers. The deeper shearing layer involves a greater fraction of the particles in inelastic collisions (and sliding contacts), and apparently, such an assembly can dissipate energy at a faster rate than a comparable depth assembly of less-elastic particles.

An unanticipated finding is the pronounced sensitivity of the velocity and character of the deeper flows to the effective stiffness of the nearly-rigid contact normal force model. Assemblies with relatively soft particles (that would result in static "overlaps" on the order of one half of one percent of a particle diameter due to the large overburden load of the deepest flows, e.g., 40 per unit area) produce dynamic loads in the rapid shearing lower layer with up to 5% of a diameter overlap. This large overlap allows the particles immediately above the bottommost rolling layer to glide over them with less vertical motion than stiffer particles experience. This results in less kinetic energy going into the layers above the bottommost rolling layer and a correspondingly thinner shearing layer and higher mean flow velocities. Increasing the stiffness by 1 or 2 orders of magnitude significantly increased the depth of the shearing layer and produced lower mean flow velocities for the flows deeper than 10 per unit area. The shallow flows (less than 5 per σ^2 area) were relatively insensitive to the stiffness of the spheres, since even the softest particles simulated only experienced dynamic overlaps of one half of one percent of a particle diameter. Further simulations and interpretation of the flows are in progress.

The flows reported here appear to differ qualitatively from the experimental flows of Johnson et al. (1990). It is not clear at this time if the perfectly flat nature of the simulated incline contributes to the differences. Future simulations will introduce various degrees of roughness for comparison with experimentally measured flows. Also, various theoretical efforts are currently underway investigating the interactions and flow behavior of inelastic and frictional particles flowing on inclined surfaces and between frictional and bumpy boundaries (Louge et al., 1991; Jenkins, 1992; Richman and Martin, 1991). It is anticipated that in the near future we will be able to directly compare simulations to kinetic-theory predictions for similar particles and boundary conditions.

Acknowledgement

This work was performed under the auspices of the US Department of Energy by the Lawrence Livermore Laboratory under Contract No. W-7405-Eng-48. Furthermore, this work was supported by the US Department of Energy, Advanced Research and Technology Development under the Solids Transport Program administered by Pittsburgh Energy Technology Center. That support is gratefully acknowledged.

References

Allen, M.P. and D.J. Tildesley (1987), *Computer Simulation of Liquids*, Clarendon Press, Oxford.

Campbell, C.S. (1986), Computer simulation of rapid granular flows, in: J.P. Lamb ed., *Proc. 10th U.S. National Congress of Applied Mechanics*, ASME, New York.

Cundall, P.A. and O.D.L. Strack (1979a), The distinct element method as a tool for research in granular media, Part II, University of Minnesota Report on NSF Grant ENG76-20711, 204 pp.

Cundall, P.A. and O.D.L. Strack (1979b), A discrete numerical model for granular assemblies, *Geotechnique 29*, 47–65.

Drake, T.G. (1988), Experimental flows of granular material, Ph.D. Dissertation, University of California, Los Angeles, 145 pp.

Drake, T.G. and O.R. Walton (1992), *Comparison of Experimental and Simulated Grain Flows*, *J. Appl. Mech.*, submitted.

Evans, D.J. (1977), *Molec. Phys. 34 (2)*, 317–325; also, Evans, D.J. and S. Murad (1977), *Molec. Phys. 34*, 327.

Jenkins, J.T. and F. Mancini (1989), Kinetic theory for binary mixtures of smooth, nearly elastic spheres, *Phys. Fluids. A 1 (12)*, 2050–2057.

Jenkins, J.T. (1992), Boundary conditions for rapid granular flows: Flat, frictional walls, *J. Appl. Mech. 59*, 120.

Johnson, P.C., P. Mott and R. Jackson (1990), Frictional. collisional equations of motion for particulate flows and their application to chutes, *J. Fluid Mech. 210*, 501–535.

Louge, M.Y., J.T. Jenkins and M.A. Hopkins (1991), Computer simulations of rapid granular shear flows between parallel bumpy boundaries, *Phys. Fluids A*, also, Computer

simulations of rapid granular flows interacting with a flat, frictional boundary, in: H. Adeli and R. Sierakowski, eds., *Mechanics Computing in 1990's and Beyond*, ASCE, New York, Vol. 2, pp. 1254–1258.

Lun, C.K.K., S.B. Savage, D.J. Jeffery and N. Chepurniy (1984), Kinetic theory for granular flow: Inelastic particles in Couette flow and slightly inelastic particles in a general flow field, *J. Fluid Mech. 140*, 223–256.

MacRae, J.C. and W.A. Gray (1961), *Br. J. Appl. Phys. 12*, 164–171.

Mindlin, R.D. (1949), Compliance of elastic bodies in contact, *J. Appl. Mech., Trans. ASME 16*, 259–268.

Owe Berg, T.G., R.L. McDonald and R.J. Trainor, Jr. (1969), *Powder Technol. 3*, 183–188.

Richman, M.W. (1989), *J. Rheol. 33 (8)*, 1293–1306.

Richman, M.W. and R.E. Martin (1991), Granular flows down bumpy inclines, *Proc. Joint U.S. DOE–NSF Workshop on Flow of Particulates and Fluids*, Worcester, MA, October 23–24, 1991, pp. 287–298, (available from U.S. Nat. Tech. Info. Service, Springfield, VA 22161).

Patton, J.S. (1985), Experimental study of shear flows and convective heat transfer characteristics of granular materials, Ph.D. Thesis, California Institute of Technology, Report No. 200.21, 160 pp.

Savage, S.B. and M. Sayed (1984), Stresses developed by dry cohesionless granular material sheared in an annular shear cell, *J. Fluid Mech. 142*, 391–430.

Trent, B.C. and O.R. Walton (1987), Private Communication, Los Alamos National Laboratory and Lawrence Livermore National Laboratory.

Walton, O.R. (1990), Computer simulation of rapidly flowing granular solids, in: S. Ishizaka, ed., *Science on Form*, KTK Scientific Publishers, Tokyo, pp. 175–189.

Walton, O.R. (1992), Numerical simulation of inelastic frictional particle–particle interactions, in: Roco, ed., *Particulate Two-Phase Flow*, Ch. 25, Butterworth–Heinemann, Boston.

Walton, O.R., and R.L. Braun (1986), *J. Rheol. 30 (5)*, 949–980.

Walton, O.R., H. Kim and A.D. Rosato (1991), Microstructure and stress differences in shearing flows, in: H. Adeli and R. Sierakowski, eds., *Mechanics Computing in 1990's and Beyond*, Vol. 2, ASCE, New York, pp. 1249–1253.

Zhang, Y. and C.S. Campbell (1992), The interface between fluid-like and solid-like behavior in two-dimensional granular beds, *J. Fluid. Mech., 237*, 541–568.